

# Pb<sub>0.4</sub>Bi<sub>1.6</sub>Sr<sub>2</sub>CaCu<sub>2</sub>O<sub>8+x</sub> and oxygen stoichiometry: Structure, resistivity, Fermi-surface topology, and normal-state properties

Jian Ma

*Department of Physics, University of Wisconsin-Madison, Madison, Wisconsin 53706  
and Applied Superconductivity Center, University of Wisconsin-Madison, Madison, Wisconsin 53706*

P. Alm eras

*Institut de Physique Appliqu ee, Ecole Polytechnique F ed erale, CH-1015 Lausanne, Switzerland*

R.J. Kelley

*Department of Physics, University of Wisconsin-Madison, Madison, Wisconsin 53706  
and Applied Superconductivity Center, University of Wisconsin-Madison, Madison, Wisconsin 53706*

H. Berger and G. Margaritondo

*Institut de Physique Appliqu ee, Ecole Polytechnique F ed erale, CH-1015 Lausanne, Switzerland*

X.Y. Cai and Y. Feng

*Applied Superconductivity Center, University of Wisconsin-Madison, Madison, Wisconsin 53706*

M. Onellion

*Department of Physics, University of Wisconsin-Madison, Madison, Wisconsin 53706  
and Applied Superconductivity Center, University of Wisconsin-Madison, Madison, Wisconsin 53706*

(Received 19 October 1994)

Pb<sub>0.4</sub>Bi<sub>1.6</sub>Sr<sub>2</sub>CaCu<sub>2</sub>O<sub>8+x</sub> [Bi(Pb)-2212] single-crystal samples were studied using transmission electron microscopy (TEM), *ab*-plane ( $\rho_{ab}$ ) and *c*-axis ( $\rho_c$ ) resistivity, and high-resolution angle-resolved ultraviolet photoemission spectroscopy (ARUPS). TEM reveals that the modulation in the *b* axis for Pb(0.4)-doped Bi(Pb)-2212 is dominantly of Pb type that is not sensitive to the oxygen content of the system, and the system clearly shows a structure of orthorhombic symmetry. Oxygen-annealed samples exhibit a much lower *c*-axis resistivity and a resistivity minimum at 80–130 K. He-annealed samples exhibit a much higher *c*-axis resistivity and  $d\rho_c/dT < 0$  behavior below 300 K. The Fermi surface (FS) of oxygen-annealed Bi(Pb)-2212 mapped out by ARUPS has a pocket in the FS around the  $\bar{M}$  point and exhibits orthorhombic symmetry. There are flat, parallel sections of the FS, about 60% of the maximum possible along  $k_x = k_y$ , and about 30% along  $k_x = -k_y$ . The wave vectors connecting the flat sections are about  $0.72(\pi, \pi)$  along  $k_x = k_y$ , and about  $0.80(\pi, \pi)$  along  $k_x = -k_y$ , rather than  $(\pi, \pi)$ . The symmetry of the near-Fermi-energy dispersing states in the normal state changes between oxygen-annealed and He-annealed samples.

## I. INTRODUCTION

For cuprate superconductors, the shape of the Fermi surface and the properties of the normal-state electronic states has been of continuing interest. The shape of the Fermi surface is of interest because it constrains theoretical models. In YBa<sub>2</sub>Cu<sub>3</sub>O<sub>7-x</sub>, excellent agreement has been obtained between angle-resolved photoemission experiments<sup>1-4</sup> and local-density approximation (LDA) band-structure calculations.<sup>5-7</sup> More recently, Gofron *et al.*<sup>8</sup> have reported an extended van Hove singularity for YBa<sub>2</sub>Cu<sub>3</sub>O<sub>7-x</sub>. Abrikosov, Campuzano, and Gofron<sup>9</sup> have argued that such a band-structure feature is important in understanding the high superconducting transition temperature ( $T_c$ ).

The symmetry of electronic states comprising the Fermi surface is identified in YBa<sub>2</sub>Cu<sub>3</sub>O<sub>7-x</sub> (Refs. 3 and 4) because the material is underdoped for  $6.35 <$

$x < 6.95$  and oxygen is removed predominantly from the chains.<sup>10-12</sup> The *c*-axis resistivity  $\rho_c$  increases as  $x$  increases, and the interlayer coupling weakens. Several reports<sup>13</sup> indicate that the chain electronic states are involved in the superconducting properties.

The situation is less clear in Bi<sub>2</sub>Sr<sub>2</sub>CaCu<sub>2</sub>O<sub>8+x</sub> (Bi-2212). Olson and colleagues observed the Fermi surface in this material that appears to be consistent with LDA calculations.<sup>14,15</sup> They have also reported the presence of an electronlike pocket around the  $(\pi, 0)$  ( $\bar{M}$ ) point for overdoped samples; the pocket was not observed after removing oxygen.<sup>16,17</sup> These results are in qualitative disagreement with a rigid-band model. Several other authors<sup>18</sup> have, on a variety of grounds, criticized the use of a rigid-band model. Further, an extended van Hove singularity along the  $\Gamma$ - $\bar{M}$ -*Z* direction in the Brillouin zone has been reported.<sup>19,20</sup> The Fermi-surface shape is not universally agreed upon, although most reports argue

that the Fermi surface exhibits orthorhombic<sup>19,21</sup> rather than tetragonal<sup>20</sup> symmetry.

$\text{Bi}_2\text{Sr}_2\text{CaCu}_2\text{O}_{8+x}$  is more complicated for three primary reasons, all material related. The BiO planes do not fit perfectly above and/or below the  $\text{CuO}_2$  planes, so a buckling in the  $\Gamma$ - $Y$  direction of the Brillouin zone results. Also, oxygen is removed or added primarily to the BiO double layer.<sup>18</sup> Since the BiO layers possess electronic states near the Fermi energy,<sup>14,15</sup> the interlayer coupling and  $\rho_c$  can be changed dramatically by varying the oxygen stoichiometry.<sup>22</sup> Finally, small differences in cation stoichiometry affect the change of oxygen stoichiometry for the same annealing conditions.<sup>18</sup>

The Pb-doped BSCCO phase has attracted much attention since Sunshine *et al.*<sup>23</sup> found that the substitution of lead can enhance the superconducting transition temperature ( $T_c$ ) in BSCCO multiphase. It was found that the lead substitution has a strong influence on the incommensurate modulation along the  $b$  axis<sup>24–29</sup> in both Bi-2212 and Bi-2223. It appears that the lead doping can reduce the structural anisotropy (ratio of  $\rho_c/\rho_{ab}$ ) (Ref. 30) which is always a factor complicating the interpretation of the experimental data.<sup>29</sup> It is generally believed that Pb doping does not perturb the electronic state critical to forming the superconducting state in this system.<sup>31</sup> Therefore the electronic structure of Bi(Pb)-2212 should be a proper representation of lead-free Bi(Pb)-2212.

We have performed extensive measurements on both oxygen-annealed and helium-annealed Bi(Pb)-2212 single crystals using transmission electron microscopy (TEM), in-plane and  $c$ -axis resistivity, and angle-resolved photoemission spectroscopy (ARUPS). We have used Bi(Pb)-2212 samples due to the larger variation in oxygen stoichiometry that we have been able to reach with single-crystal samples.

Our data in this paper lead to several conclusions for Bi(Pb)-2212: Bi(Pb)-2212 is structurally orthorhombic; adding oxygen is very effective in decreasing the  $c$ -axis resistivity, and quite possibly changing the interlayer coupling; the Fermi surface exhibits orthorhombic symmetry, incomplete Fermi-surface nesting, and, for sufficiently overdoped samples, a pocket around the  $\bar{M}$  point in the Brillouin zone; the symmetry of the electronic states comprising the Fermi surface changes with oxygen stoichiometry; the rigid-band model does not apply.

## II. EXPERIMENT

The single-crystal samples of  $\text{Bi}_{1.6}\text{Pb}_{0.4}\text{Sr}_2\text{CaCu}_2\text{O}_{8+x}$  [Bi(Pb)-2212] were prepared using the standard self-flux method.<sup>32</sup> The crystals were characterized using four-point resistivity, ac susceptibility, x-ray diffraction, and transmission electron microscopy.

Transmission electron microscopy measurements were carried out with a JEOL 200CX microscope operating at 200 kV. The Bi(Pb)-2212 single-crystal samples were cleaved repeatedly and thin flakes were then mounted on a single-hole gold grid using  $M$ -bond adhesive. In order to study the structural modulation from the [100] direction, the crystals were mounted so that the sample

foil surface is perpendicular to the [100] direction. The samples were then mechanically polished and finally ion milled at 4.5 kV.

The ARUPS experiments were performed using the four-meter normal-incidence monochromator at the Wisconsin Synchrotron Radiation Center in Stoughton, WI. The beamline provides highly ( $> 95\%$ ) linearly polarized light with the photon electric vector in the horizontal plane and with photon energy resolution better than 10 meV. The angle-resolved photoemission chamber includes a reverse-view low-energy electron diffraction (LEED) optics used to orient the sample *in situ* after cleaving. The electron energy analyzer is a 50 mm Vacuum Science Workshop (VSW) hemispherical analyzer mounted on a two axis goniometer, with an acceptance full angle of  $2^\circ$ . The base pressure is  $6 \times 10^{-11}$  torr. The incidence angle between the photon Poynting vector and surface normal was  $45^\circ$  unless otherwise noted.

For photoemission studies, the samples were transferred from a load lock chamber with a base pressure of  $5 \times 10^{-9}$  torr to the main chamber, and cleaved at 30 K in a vacuum of  $6\text{--}8 \times 10^{-11}$  torr. The sample holder includes the capability to rotate the sample, at low temperatures, *in situ* about the surface normal for precision alignment with respect to the photon electric field. To measure the normal-state electronic band structure, the temperature was raised above  $T_c$  to 95 K. The stability of the temperature was  $\pm 1$  K. For this study, the overall energy resolution employed was 55 meV unless otherwise stated.

For a quasi-two-dimensional system such as  $\text{Bi}_2\text{Sr}_2\text{Ca}_1\text{Cu}_2\text{O}_{8+x}$  the initial state of the electron can be determined by measuring the component of the electron momentum parallel to the sample surface ( $\mathbf{k}_\parallel$ ). By measuring the energy distribution curves (EDC's) for different directions ( $\theta, \phi$ ) of the emitted photoelectron relative to the surface normal, the  $\mathbf{k}_\parallel$  of the initial state is derived from the relation  $\mathbf{k}_\parallel = 0.512 \text{ \AA}^{-1} \sqrt{E_{\text{kin}}} (\sin \theta \cos \phi \hat{k}_x + \sin \phi \hat{k}_y)$ , where  $E_{\text{kin}}$  is the kinetic energy of measured photoelectrons in the unit of eV and  $\hat{k}_x$  and  $\hat{k}_y$  denote unit vectors along horizontal and vertical directions, respectively. A freshly *in situ* deposited gold film was used as a reference to determine the Fermi energy.

The modified modulation structure in Bi(Pb)-2212 due to lead substitution was confirmed by our *in situ* LEED study. At low electron-beam energy (27 eV) the LEED pattern exhibited an almost  $1 \times 1$  structure for Bi(Pb)-2212, whereas it was a  $4.6 \times 1$  pattern for lead-free Bi-2212. At higher electron-beam energies (above 40 eV) we do observe a modulation for the oxygen-annealed samples that is absent for the He/Ar-annealed samples. The sharp and intense LEED spots confirmed the high quality of the cleaved surfaces which is a prerequisite for performing ARUPS measurements.

## III. CRYSTAL STRUCTURAL AND TRANSPORT MEASUREMENTS

### A. Crystal structure of Bi(Pb)-2212

The chemical composition and the crystal structure of the Pb-doped Bi-2212 single crystals were examined

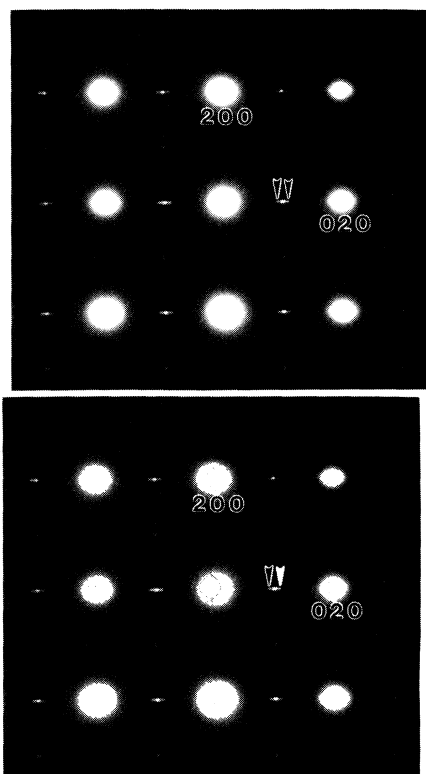


FIG. 1. The [001] (a) and [100] (b) electron-diffraction patterns (EDP) of the oxygen-annealed Bi(Pb)-2212 single-crystal samples. Diffraction spots are indexed based on the fundamental structure. Satellite spots, as indicated by arrows, are due to the modulated structure. Similar EDP were observed on the helium-annealed Bi(Pb)-2212 single-crystal samples.

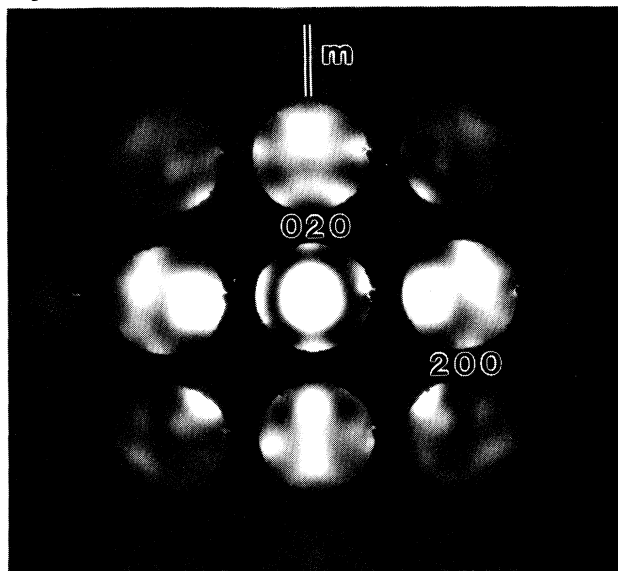


FIG. 2. [001] Convergent beam electron-diffraction (CBED) pattern of the oxygen-annealed Bi(Pb)-2212 single-crystal samples. The pattern has only one mirror plane as indicated by the vertical line marked  $m$ , implying a  $2mm$  point-group symmetry of orthorhombic structure. A similar CBED pattern was observed on the helium-annealed Bi(Pb)-2212 single-crystal samples.

by analytical electron microscopy. Energy dispersive x-ray spectroscopy confirmed that the Pb was incorporated into the Bi-2212 crystals. A twinlike domain structure was observed in the Bi(Pb)-2212 crystals. This is rarely seen in the lead-free crystals. Figure 1 shows the [001] (a) and [100] (b) diffraction patterns of oxygen-annealed Bi(Pb)-2212 crystals. Both patterns show the modulated structure in the Bi system. The modulation can be understood in terms of a basic structure (shown as the indexed strong main spots) plus a superimposed displacement field (shown by the satellite spots

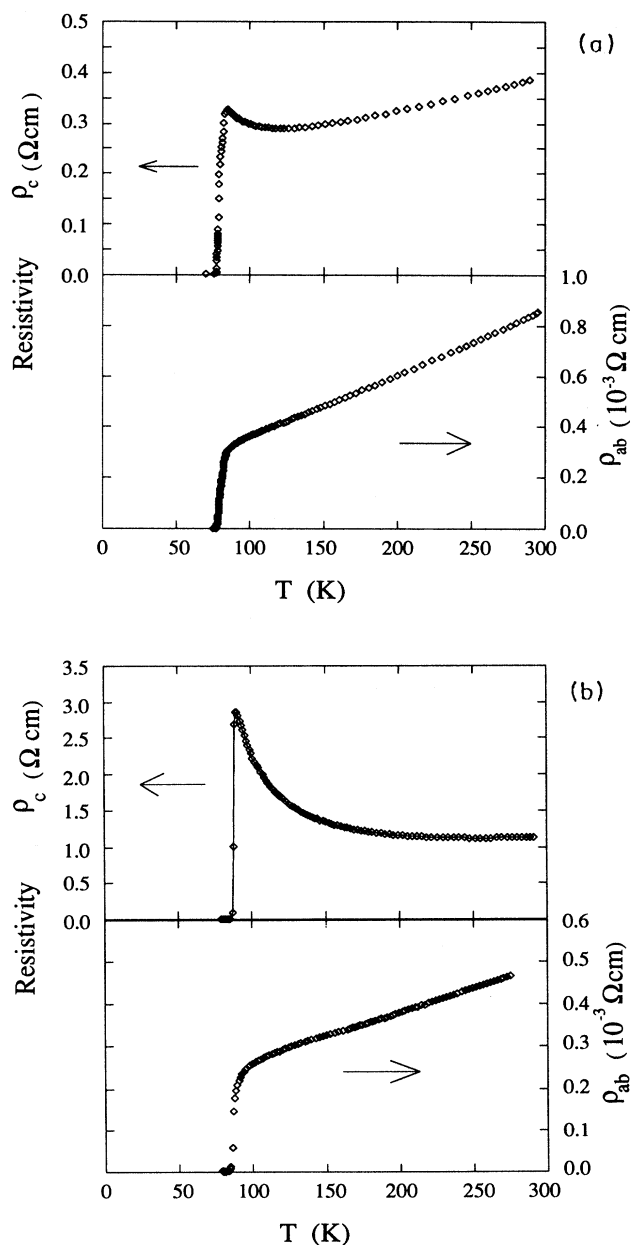


FIG. 3. Temperature dependence of the  $c$ -axis resistivity and in-plane resistivity for Bi<sub>1.6</sub>Pb<sub>0.4</sub>Sr<sub>2</sub>CaCu<sub>2</sub>O<sub>8+x</sub> single crystals (a) annealed in one atmosphere O<sub>2</sub> at 600 °C for 1 h; (b) annealed in one atmosphere helium at 600 °C for 1 h.

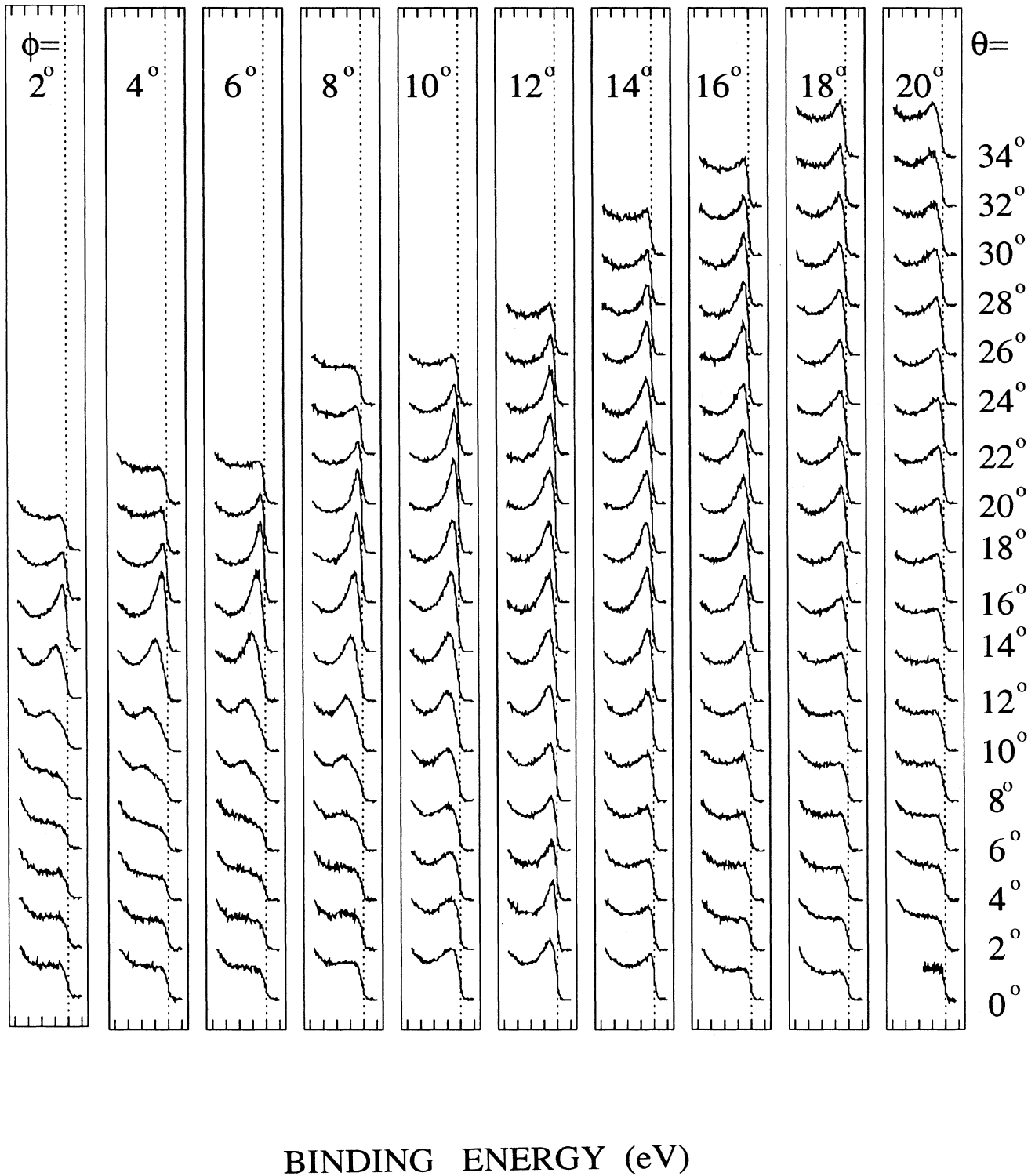


FIG. 4. The normal-state ( $T = 95$  K) angle-resolved photoemission spectra (EDC) measured on an oxygen overdoped  $\text{Bi}_{1.6}\text{Pb}_{0.4}\text{Sr}_2\text{CaCu}_2\text{O}_{8+x}$  single-crystal sample of  $T_c = 75$  K using photon energy  $h\nu = 21$  eV. The photoelectron emission angle relative to the surface normal ( $\theta$  and  $\phi$ ) are marked. The spectra in each vertical column were taken by changing the angle  $\theta$  with fixed angle  $\phi$ . The data were taken in the range  $0 \leq \phi \leq 20^\circ$  and  $0 \leq \theta \leq 40^\circ$  which covers almost  $2/3$  of the first Brillouin zone.

marked by arrows). The [100] pattern shows only one type of modulation which is exactly parallel with the  $b$  direction. This is the typical Pb-type modulation discussed previously.<sup>25–27</sup> However, the modulation wavelength along the  $b$  direction is about  $13b$ , much longer than reported previously (typically 8–10 $b$ ).<sup>33–35</sup> Such an increase of the modulation wavelength may be related to the Pb content and the oxygenation effect. No Bi-type modulation<sup>25–27</sup> was observed in this sample.

In order to identify the structural symmetry of the crystals, we have performed convergent beam electron-diffraction (CBED) measurements. Care was paid to avoid any imperfect area when selecting regions to perform CBED measurements, since any defects or artifacts can break the true crystal symmetry.<sup>36</sup> CBED were performed many times at different locations in the crystals and Fig. 2 shows a typical example of the [001] CBED patterns obtained from the oxygen-annealed sample. It is evident that only one mirror plane can be identified, as indicated by the vertical line marked with  $m$ , implying a  $2mm$  point-group symmetry of the orthorhombic system.

In a comparative study, we have performed the same CBED study on a Pb-free Bi-2212 single crystal and found that there are two mirror planes in the [001] pattern, implying a  $mmm$  symmetry group, which also belongs to the orthorhombic structure. Therefore, it seems that the Pb-doping lowers the symmetry of the 2212 crystal. To date, reports on the precise symmetry of the Bi(Pb)-2212 system have not reached a consensus.<sup>34,37</sup> Nevertheless, it is agreed that the structure of the Bi(Pb)-2212 studied here exhibits orthorhombic, not tetragonal, symmetry.

We also performed the same experiments on the helium-annealed Bi(Pb)-2212 samples. Again, no Bi-type modulation was observed. The Pb-type modulation remained unchanged as compared to the modulation observed in the oxygen-annealed samples. This suggests that the change of the oxygen content does not affect the Pb-type modulation, which is consistent with the results reported by Chen *et al.*<sup>26,27</sup> in their Pb-doped bulk 2212 samples. No noticeable changes were found in crystal symmetry in comparison to the oxygen-annealed samples. Only one mirror plane was observed in the [001] CBED pattern, similar to the results for the oxygen-annealed sample.

### B. In-plane and $c$ -axis resistivity

For lead-free Bi-2212, the in-plane resistivity is metallic and the out-of-plane resistivity is highly semiconducting.<sup>38</sup> The resistivity anisotropy ratio of  $\rho_c/\rho_{ab}$  near  $T_c$  varies from  $\sim 2 \times 10^5$  (lead-free, vacuum-annealed) to  $\sim 800$  (lead-doped, oxygen-annealed).<sup>38,39</sup> Transport measurements of the in-plane and  $c$ -axis resistivity were first performed on Bi(Pb)-2212 single-crystal samples by Régi and co-workers.<sup>30</sup> They demonstrated that lead substitution reduced the resistivity anisotropy ratio  $\rho_c/\rho_{ab}$  by two orders of magnitude near the transition temperature  $T_c$ , compared to the lead-free Bi-2212.

Furthermore, they showed that the  $c$ -axis resistivity behavior becomes metallic for lead-doped 2212. Our resistivity measurements on oxygen-annealed Bi(Pb)-2212 fully confirm their results, as shown in Fig. 3(a). A linear behavior of  $\rho_c$  occurs in the temperature range of 125–300 K. The upward curvature near  $T_c$  suggests  $c$ -direction localization of carriers.

However, as shown in Fig. 3(b), for He annealed Bi(Pb)-2212 we see similar semiconducting behavior in the  $c$ -axis transport as is found for lead-free 2212. X-ray diffraction, TEM, and LEED measurements showed no significant structural difference between He-annealed and O<sub>2</sub>-annealed lead-doped samples. These data are thus a strong indication that it is the amount of oxygen incorporated into a Bi(Pb)-2212 sample that controls the  $c$ -axis transport properties. The presence of lead makes it easier to get oxygen into or out of Bi(Pb)-2212 samples. As we will show in the next section, O<sub>2</sub> doping changes both the carrier concentration in Bi(Pb)-2212 (in turn changing the chemical potential), and the electronic structure.

### IV. FERMI-SURFACE TOPOLOGY

The topology of the Fermi surface is an important measure of the electronic structure. The Fermi surface has

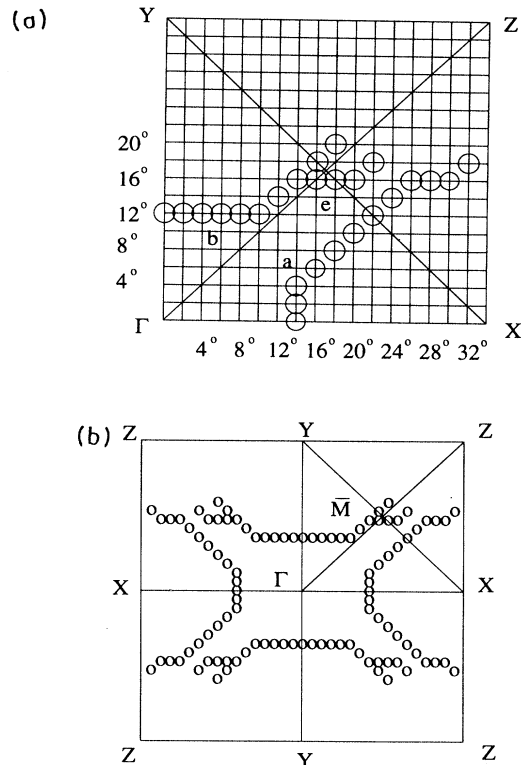


FIG. 5. (a) The experimentally determined Fermi surface of Bi(Pb)-2212 from EDC measurements using  $h\nu = 21$  eV. The data were taken on 160 points in the first Brillouin zone. No symmetry assumption is used. All of the data points are experimental ones. (b) The Fermi surface of Bi(Pb)-2212 constructed out of experimental data points and assumption of  $C_{2v}$  symmetry.

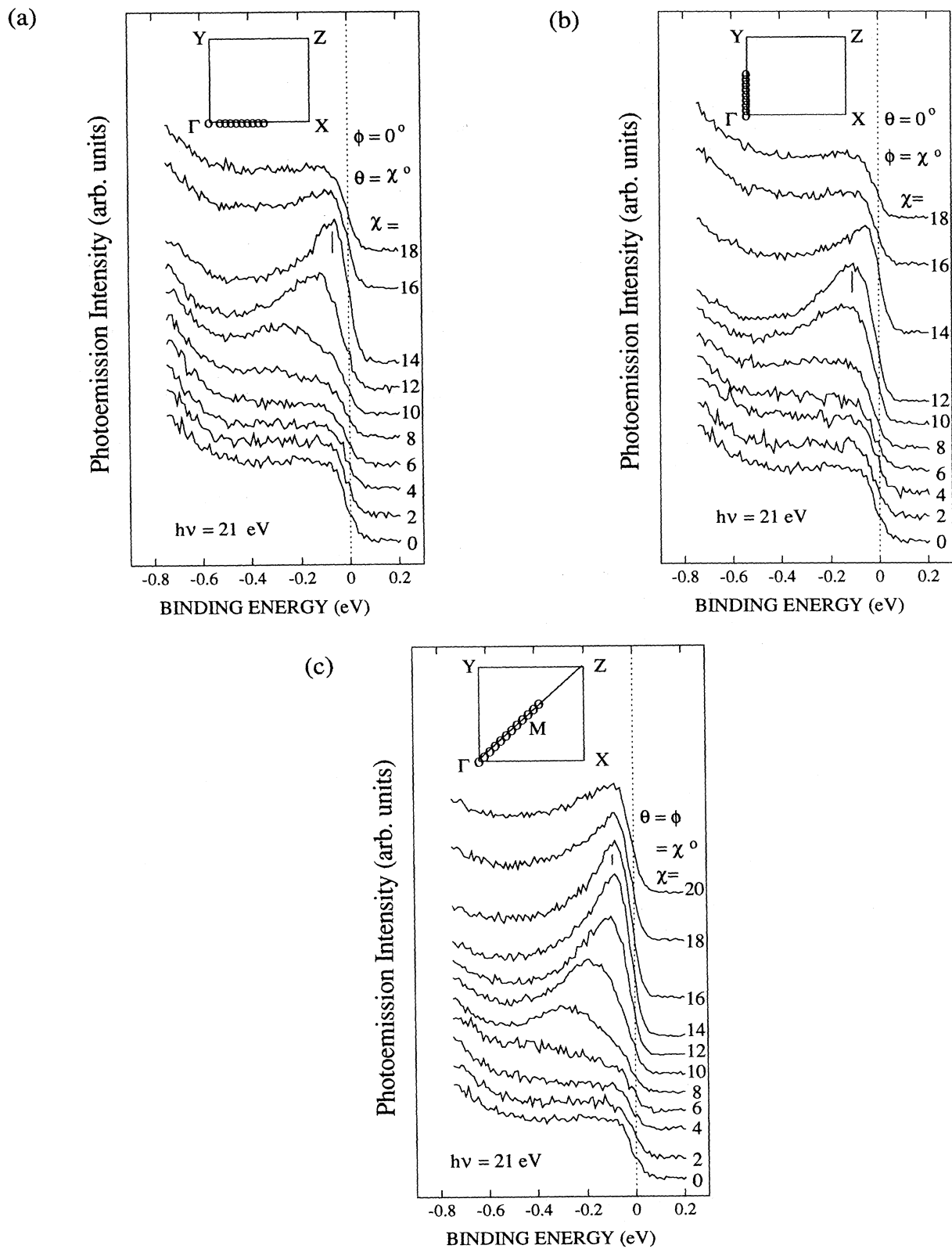


FIG. 6. Normal-state ( $T = 95$  K) angle-resolved photoemission spectra for an oxygen overdoped  $\text{Bi}_{1.6}\text{Pb}_{0.4}\text{Sr}_2\text{CaCu}_2\text{O}_{8+x}$  single crystal of  $T_c = 75$  K along (a) the  $\Gamma$ -X direction; (b) the  $\Gamma$ -Y direction; (c) the  $\Gamma$ -M-Z direction. The photon energy employed was 21 eV. The insets show the locations in the first Brillouin zone where the data were taken.

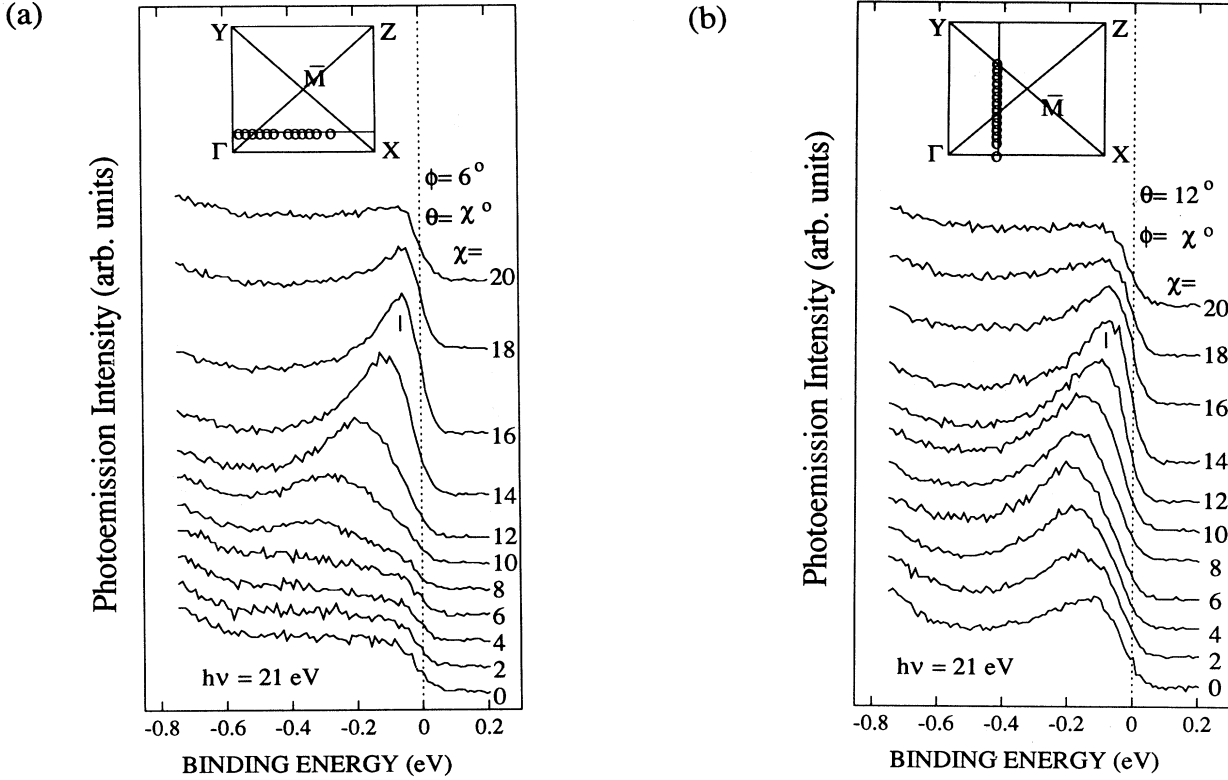


FIG. 7. Normal-state ( $T = 95$  K) angle-resolved photoemission spectra for an oxygen overdoped  $\text{Bi}_{1.6}\text{Pb}_{0.4}\text{Sr}_2\text{CaCu}_2\text{O}_{8+x}$  single crystal of  $T_c = 75$  K along (a) a direction parallel to  $\Gamma$ - $X$  at  $\phi = 6^\circ$ , where the Fermi-surface crossing happens at  $\theta = 16^\circ$  instead of  $\theta = 14^\circ$  for  $\phi < 6^\circ$ ; (b) a direction parallel to  $\Gamma$ - $Y$  at  $\theta = 12^\circ$ , where the Fermi-surface crossing is at  $\phi = 14^\circ$  instead of  $\phi = 12^\circ$  for  $\theta < 12^\circ$ .

been mapped out on lead-free  $\text{Bi}_2\text{Sr}_2\text{CaCu}_2\text{O}_{8+x}$  (Bi-2212) in different oxygen-doped regimes using ARUPS by different groups.<sup>14,19,40,20</sup> Unlike what has been done for  $\text{YBa}_2\text{Cu}_3\text{O}_{7-x}$  (YBCO-123),<sup>2-4</sup> there has not yet been a *systematic* study of the Fermi surface versus oxygen stoichiometry for the Bi-2212 systems. We believe that the difficulty in obtaining totally consistent results from different research groups stems from the lack of control of oxygen stoichiometry compared to that available for the YBCO-123 system.

Due to the comparative ease with which the oxygen stoichiometry can be varied, the  $\text{Bi}_{1.6}\text{Pb}_{0.4}\text{Sr}_2\text{CaCu}_2\text{O}_{8+x}$  [Bi(Pb)-2212] system appears to be an ideal system to study the Fermi-surface topology. Figure 4 presents the complete set of angle-resolved photoemission spectra taken on the same oxygen overdoped  $\text{Bi}_{1.6}\text{Pb}_{0.4}\text{Sr}_2\text{CaCu}_2\text{O}_{8+x}$  single-crystal sample. A photon energy of  $h\nu = 21$  eV was used. The sample was oriented so that the  $\Gamma$ - $X$  is in the horizontal plane which is also the photon polarization plane. The effect of polarization on the different orientations of the sample was very useful in determining the symmetries of the normal-state bands as will be discussed in the next section.

In Fig. 4, the spectra in each vertical column were obtained by changing the angle  $\theta$  with fixed angle  $\phi$ . The spectra have been aligned horizontally so that the spectra taken at the same  $\theta$  angle, but at different  $\phi$  angles are on the same horizontal level. By keeping  $\theta$  fixed, one

can go along a direction parallel to the  $\Gamma$ - $Y$  symmetry direction. Similarly, one can go along a direction parallel to the  $\Gamma$ - $X$  direction by scanning  $\theta$  with  $\phi$  fixed. We shall discuss some of the spectra in detail, below.

Using the data of Fig. 4, a purely empirical construction of the Fermi surface of  $\text{O}_2$ -annealed  $\text{Bi}_{1.6}\text{Pb}_{0.4}\text{Sr}_2\text{CaCu}_2\text{O}_{8+x}$  is illustrated in Fig. 5(a). We emphasize that no *a priori* symmetry assumptions were made in constructing Fig. 5(a). The Fermi surface is orthorhombic, and  $\Gamma$ - $X$  and  $\Gamma$ - $Y$  are inequivalent.<sup>19,21,41,40</sup> Specifically, the shape of the Fermi surface around the  $X$  point is very similar to that reported by Aebi *et al.*<sup>40</sup> We do not have conclusive data to comment on the presence or absence of the “shadow bands” reported by Aebi *et al.*<sup>40</sup> However, again similar to Ref. 40, the Fermi-surface nesting is not complete. Instead, the portion of the Fermi surface parallel to  $\Gamma$ - $X$  ( $k_x = k_y$ ) is about 60% of the extent expected for perfect nesting, and the nesting wave vector is approximately  $0.72(\pi, \pi)$ . The portion of the Fermi surface parallel to  $\Gamma$ - $Y$  ( $k_x = -k_y$ ) is about 30% of the extent expected for perfect nesting, and the nesting wave vector is approximately  $0.80(\pi, \pi)$ .

The above aspects are illustrated more explicitly in Fig. 5(b). We have assumed only  $C_{2v}$  symmetry in constructing Fig. 5(b). Our nesting wave vectors can be directly compared to the predictions of Ruvald, Rieck, and Virosztek<sup>42</sup> which predict a marked decrease in the superconducting transition temperature ( $T_c$ ) when the

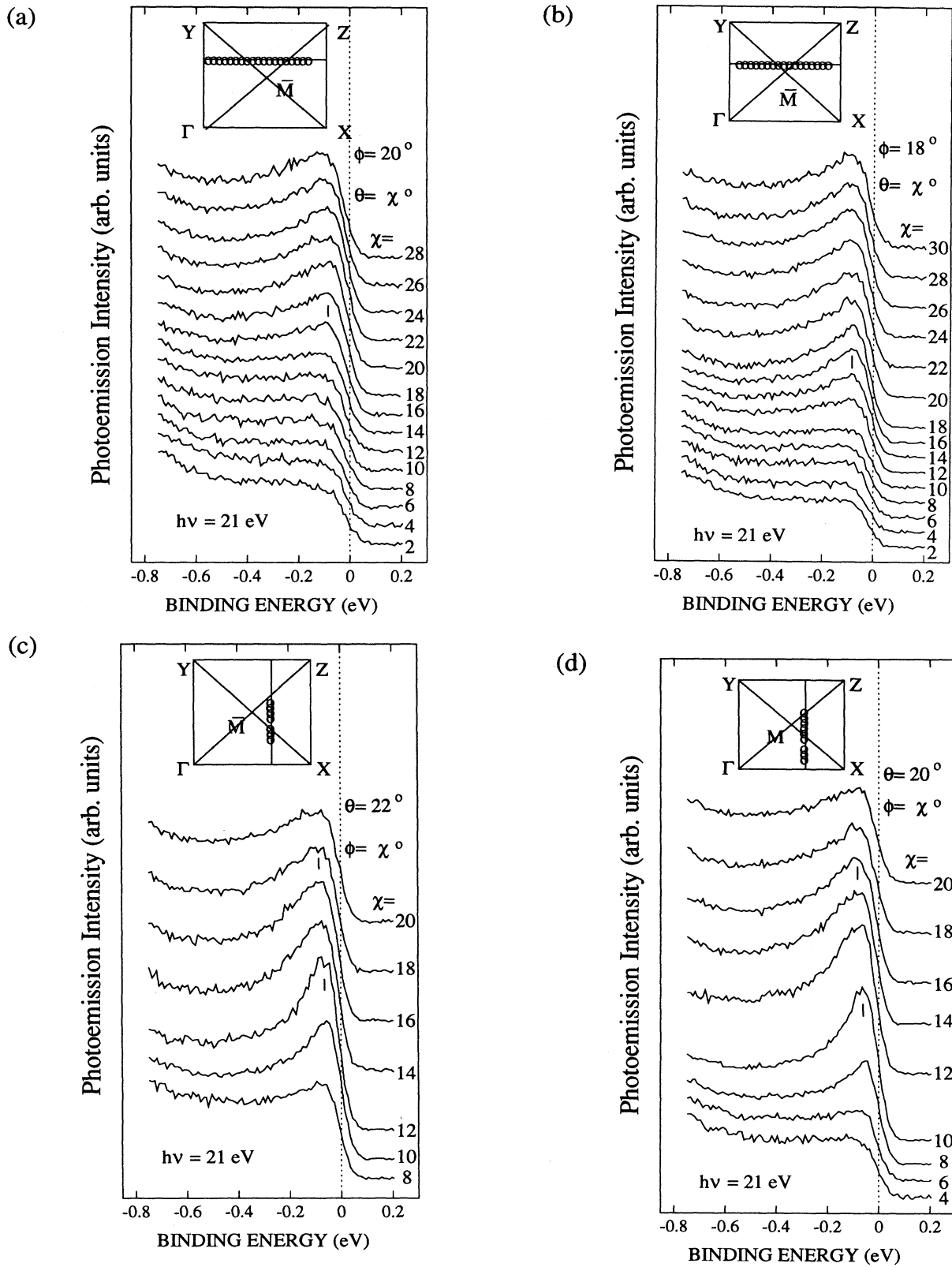


FIG. 8. Normal-state ( $T = 95$  K) angle-resolved photoemission spectra for an oxygen overdoped  $\text{Bi}_{1.6}\text{Pb}_{0.4}\text{Sr}_2\text{CaCu}_2\text{O}_{8+x}$  single crystal of  $T_c = 75$  K along the directions parallel to  $\Gamma$ - $X$  (a) at  $\phi = 20^\circ$ ; (b) at  $\phi = 18^\circ$ , and the directions parallel to  $\Gamma$ - $Y$  (c) at  $\theta = 22^\circ$ ; (d) at  $\theta = 20^\circ$ ; and (e) at  $\theta = 18^\circ$ . The pocketlike Fermi surface around  $M$  is derived from those cuts.

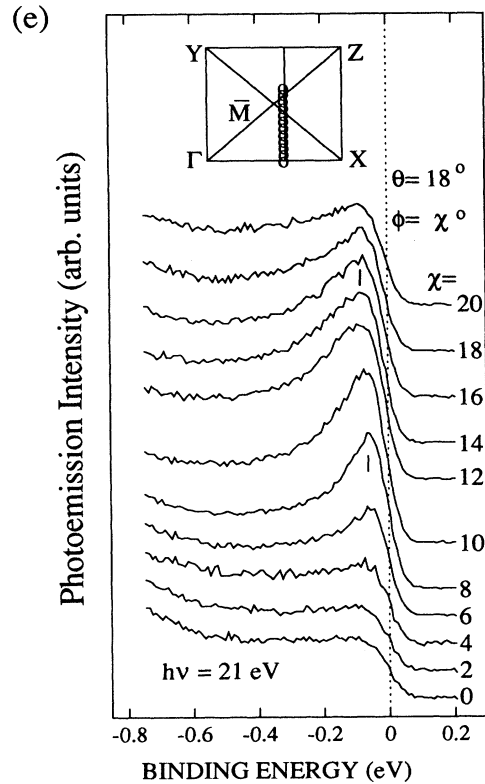


FIG. 8. (Continued).

nesting wave vector decreases from  $(\pi, \pi)$ . Our results agree qualitatively with Ref. 42: the  $T_c = 75$  K of O<sub>2</sub>-annealed Bi(Pb)-2212 is lower than the  $T_c = 90$  K of optimally doped Bi-2212. However, their predicted  $T_c$  for our samples is below 5 K, compared to a measured value of 75 K.

In addition, our data indicate a pocket around the  $\bar{M}$  point, similar to that reported on O<sub>2</sub>-annealed Bi-2212 samples by Olson and colleagues.<sup>16</sup> The portion parallel to  $\Gamma$ -X [labeled “b” in Fig. 5(a)] merges with this pocket, while the portion around the X point [labeled “a” in Fig. 5(a)] remains distinct from the pocket. These results further indicate that  $\Gamma$ -X and  $\Gamma$ -Y are inequivalent.

To validate the Fermi surface presented in Fig. 5, we present detailed spectra along particularly important directions. Figure 6(a) illustrates the spectra taken along  $\Gamma$ -X direction. A band disperses towards the Fermi energy ( $E_f$ ) from more than 200 meV below  $E_f$  at  $\theta$  of 10° and crosses the Fermi level at  $\theta = 14^\circ$  (note abrupt reduction of photoemission intensity). Along the  $\Gamma$ -Y direction, as illustrated in Fig. 6(b), we observe an almost equally strong band dispersing towards  $E_f$ . The band crossed the Fermi energy at  $\phi = 12^\circ$ . The absolute positions of crossing are slightly different with respect to the  $\Gamma$  point between  $\Gamma$ -X and  $\Gamma$ -Y directions, indicating that the Fermi surface around the X point might be further away from  $\Gamma$  than the Fermi surface around the Y point. The difference of 2° is right at our combined experimental angular uncertainty.

The spectra along the  $\Gamma$ - $\bar{M}$  direction are illustrated

in Fig. 6(c). A band with small dispersion is observed near  $E_f$  and crosses the Fermi energy at  $\theta/\phi = 16^\circ/16^\circ$  (note reduction in photoemission intensity). We did not observe such a Fermi-surface crossing for the lead-free samples.<sup>19</sup>

The spectra indicating the turning points where the flat sections of the Fermi surface (FS) around X and Y start to curve are presented in Fig. 7. In Fig. 7, the FS crossing happened at  $\theta = 16^\circ$  for  $\phi = 6^\circ$ , whereas the FS crossings were at  $\theta = 14^\circ$  for  $\phi < 6^\circ$ . Along the direction parallel to  $\Gamma$ -Y at  $\theta = 12^\circ$ , the FS crossing was at  $\phi = 14^\circ$ , and the flat sections of FS were at  $\phi = 12^\circ$  with  $\theta < 14^\circ$ .

The evidence of the existence of the pocketlike Fermi surface is shown in Fig. 8. For a direction parallel to  $\Gamma$ -X, at  $\phi = 20^\circ$ , a band emerges from above the Fermi energy at about  $\theta = 18^\circ$  [Fig. 8(a)], with increasing photoemission intensity as the state disperses below  $E_f$ . At  $\phi = 18^\circ$ , a similar Fermi-surface crossing was observed at  $\theta = 16^\circ$  in Fig. 8. We already know [Fig. 6(c)] that there is a FS crossing at  $\phi/\theta = 16^\circ/16^\circ$ . Figure 8(c) shows two FS crossings as one goes along a direction parallel to  $\Gamma$ -Y at  $\theta = 22^\circ$ . The first crossing at  $\phi = 12^\circ$  belongs to the FS around the X point. There is also a second crossing, at  $\phi = 18^\circ$ , that is part of the pocket and not part of the FS around the Y point. The double FS crossings are also present in Fig. 8(d). The first FS crossing at  $\phi = 10^\circ$  corresponds to the FS around X point, and the second FS crossing at  $\phi = 16^\circ$  is near  $\bar{M}$  but away from Y point. Finally, in Fig. 8(e), the first FS crossing

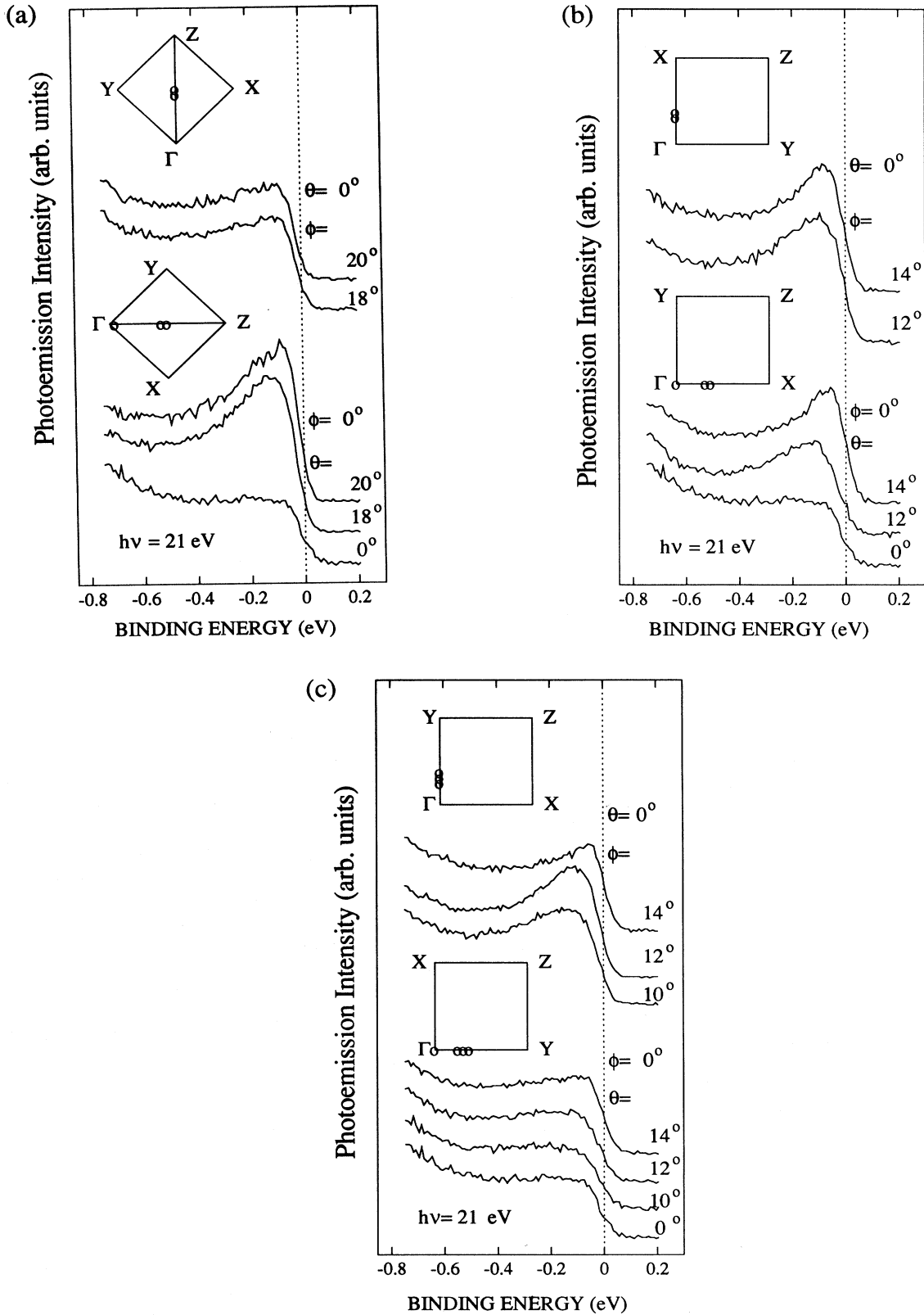


FIG. 9. Normal-state ( $T = 95$  K) angle-resolved photoemission spectra for an  $\text{O}_2$ -annealed  $\text{Bi}_{1.6}\text{Pb}_{0.4}\text{Sr}_2\text{CaCu}_2\text{O}_{8+x}$  single crystal of  $T_c = 75$  K for different geometries of photon polarization vector and crystalline orientation. (a)  $\Gamma$ - $\bar{M}$ - $Z$  is horizontal or vertical; (b)  $\Gamma$ - $X$  is horizontal or vertical; (c)  $\Gamma$ - $Y$  is horizontal or vertical. The photon polarization vector is always in the horizontal plane. The insets show the locations in the Brillouin zone where the spectra were obtained.

at  $\phi = 8^\circ$  belongs to the FS around  $X$  point and the second crossing at  $\phi = 16^\circ$  completes the pocketlike Fermi surface as indicated in Fig. 5. It was unfortunate that we were not able to take data beyond  $\phi = 20^\circ$  due to technical limitations of our sample holder arrangement, but the pocketlike FS, although incomplete, is clearly present in the spectra in Fig. 8.

In summary, the Fermi-surface map (Fig. 5) and supporting data (Figs. 4, 6–8) establish several important points: the Fermi surface exhibits orthorhombic symmetry; the Fermi-surface nesting is quite incomplete for these HTSC's ( $T_c = 75$  K); and there is a pocket around the  $M$  point. Because we observe no Fermi-surface crossing along  $\Gamma\text{-}\bar{M}\text{-}Z$  for He-annealed samples, the data indicate that there is no pocket around the  $\bar{M}$  point for He-annealed samples. Thus, insofar as a pocket is concerned, the Bi(Pb)-2212 behaves in the same qualitative fashion as reported by Olson and colleagues<sup>16,17</sup> for Bi-2212.

There are at least two models that view the “flat band” around the  $M$  point as important: Abrikosov's argument<sup>9</sup> about the effects of an extended van Hove singularity, and the Dagotto, Nazarenko, and Boninsegni<sup>43</sup> electron correlation model. The model of Dagotto, Nazarenko, and Boninsegni<sup>43</sup> achieves quanti-

tative agreement with our data on Bi-2212 samples.<sup>19</sup> To date, we are unaware of published calculations that predict the effects of a pocket on the superconducting properties. It is clear, however, that such a fundamental change in the Fermi-surface topology can serve as a test for the above models when calculations are available. Let us now turn to the second part of this report, the symmetry of the normal-state wave functions.

#### V. SYMMETRY OF THE NORMAL STATES: BLOCH'S THEOREM APPLIES

In this section, we present data demonstrating that the symmetry of the normal-state wave functions changes with oxygen stoichiometry for Bi(Pb)-2212 samples. Because Bloch's theorem applies, and x-ray-diffraction, TEM, and LEED measurements indicate no structural change in the CuO<sub>2</sub> planes, there are very few plausible explanations for the data; these are discussed after the data are presented.

We employ a standard photoemission method,<sup>44</sup> using linearly polarized light to probe the symmetry of the normal state. A photoemission process can be described as a transition of the electron from the initial state  $|\Psi_i\rangle$  to

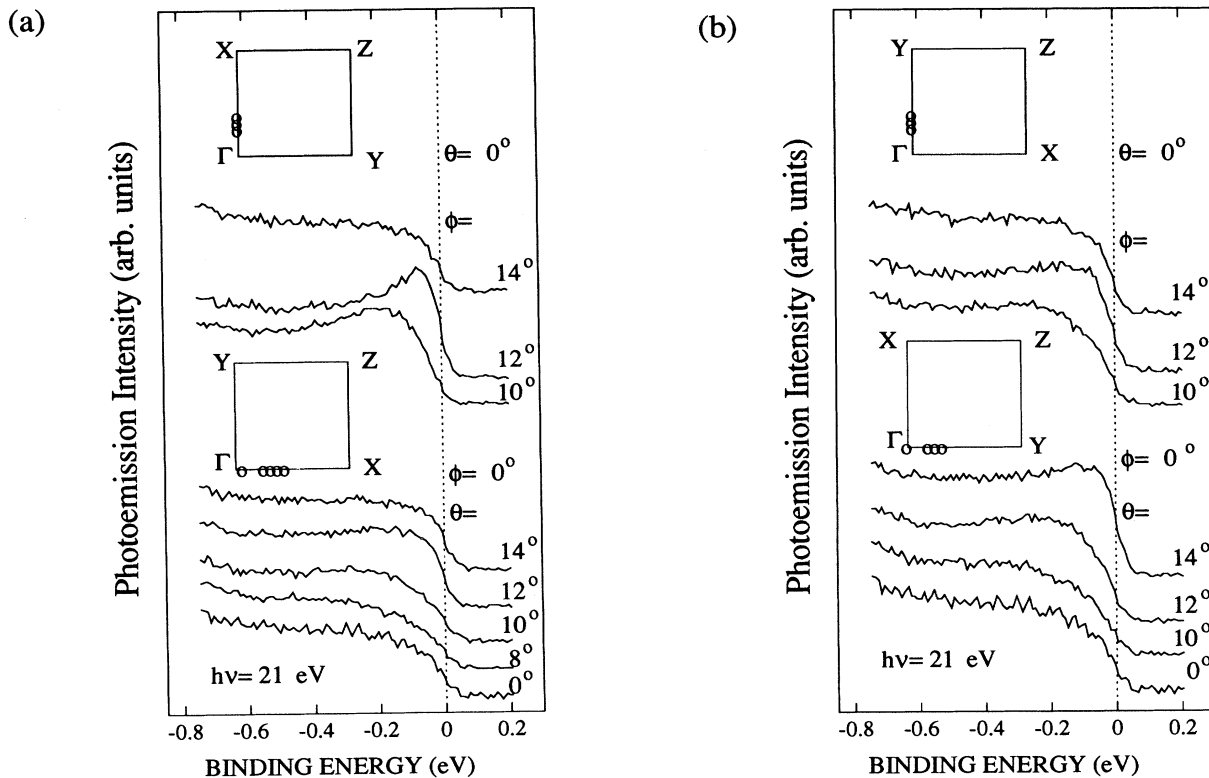


FIG. 10. Normal-state ( $T = 95$  K) angle-resolved photoemission spectra for a helium-annealed Bi<sub>1.6</sub>Pb<sub>0.4</sub>Sr<sub>2</sub>CaCu<sub>2</sub>O<sub>8-x</sub> single crystal of  $T_c = 85$  K for different geometries of photon polarization vector and crystalline orientation. For the orientation that  $\Gamma\text{-}\bar{M}\text{-}Z$  is horizontal or vertical, the spectra are similar to Fig. 9(a). However, the signals observed are quite different for the orientations (a)  $\Gamma\text{-}X$  is horizontal or vertical; (b)  $\Gamma\text{-}Y$  is horizontal or vertical. The insets show the locations in the Brillouin zone where the spectra were taken.

TABLE I. A list of possible  $s$ ,  $p$ , or  $d$  symmetries of the normal-state with orientations for which a normal-state band along  $\Gamma$ - $\bar{M}$ - $Z$  and  $\Gamma$ - $X$  could (Yes) or could not (No), by symmetry, be observed.

Orientation operation symmetry	$\Gamma$ - $\bar{M}$ - $Z$		$\Gamma$ - $X$	
	Horizontal $y \rightarrow -y$	Vertical $y \rightarrow -y$	Horizontal $x \leftrightarrow -y$	Vertical $x \leftrightarrow -y$
$s$	$\langle e e e \rangle$ Yes	$\langle e o e \rangle$ No	$\langle e e e \rangle$ Yes	$\langle e o e \rangle$ No
$p_x$	$\langle e e e \rangle$ Yes	$\langle e o e \rangle$ No	$\langle e e e+o \rangle$ Yes	$\langle e o e+o \rangle$ Yes
$p_y$	$\langle e e o \rangle$ No	$\langle e o o \rangle$ Yes	$\langle e e e+o \rangle$ Yes	$\langle e o e+o \rangle$ Yes
$p_z$	$\langle e e e \rangle$ Yes	$\langle e o e \rangle$ No	$\langle e e e \rangle$ Yes	$\langle e o e \rangle$ No
$d_{xy}$	$\langle e e o \rangle$ No	$\langle e o o \rangle$ Yes	$\langle e e e \rangle$ Yes	$\langle e o e \rangle$ No
$d_{x^2-y^2}$	$\langle e e e \rangle$ Yes	$\langle e o e \rangle$ No	$\langle e e o \rangle$ No	$\langle e o o \rangle$ Yes
$d_{3z^2-r^2}$	$\langle e e e \rangle$ Yes	$\langle e o e \rangle$ No	$\langle e e e \rangle$ Yes	$\langle e o e \rangle$ No
$d_{yz}$	$\langle e e o \rangle$ No	$\langle e o o \rangle$ Yes	$\langle e e e+o \rangle$ Yes	$\langle e o e+o \rangle$ Yes
$d_{xz}$	$\langle e e e \rangle$ Yes	$\langle e o e \rangle$ No	$\langle e e e+o \rangle$ Yes	$\langle e o e+o \rangle$ Yes
Experiment				
O <sub>2</sub> Bi(Pb)-2212	Yes	No	Yes	Yes
He Bi(Pb)-2212	Yes	No	No	Yes

a free electron final state  $|\Psi_f\rangle$  in vacuum. The differential photoionization cross section, to which the photoemission signal is proportional, can be derived from the Fermi-golden-sum rule as<sup>44</sup>

$$\frac{d\sigma}{d\Omega} \propto |\langle \Psi_f | \mathbf{P} \cdot \mathbf{A}_0 | \Psi_i \rangle|^2 \delta(E_f - E_i - h\nu), \quad (5.1)$$

where  $\mathbf{P}$  is the momentum operator and  $\mathbf{A}_0$  the vector potential of photon electric field of the energy  $h\nu$ . We define a plane of reflection symmetry by the  $z$  axis (the surface normal) and the photoelectron emission direction. In order to detect a signal, the final state of the photoelectron must be even under reflection about this symmetry plane. Otherwise, there would be a node in the final-state wave function in the symmetry plane and no signal would be observed under any condition. In our experimental setup, if the  $\mathbf{A}$  is in the  $x$  direction, or  $\mathbf{A} = A_x \hat{x}$ , the dipole operator  $\mathbf{P} \cdot \mathbf{A} = P_x A_x$  will be even under the reflection about  $xz$  plane ( $y \rightarrow -y$ ), and odd under the reflection through the  $yz$  plane ( $x \rightarrow -x$ ). By

analyzing the parities of the initial state of various possible spherical harmonics,  $s$ ,  $p$ , and  $d$ , under the same reflection operation, and comparing the  $\langle \Psi_f | \mathbf{P} \cdot \mathbf{A} | \Psi_i \rangle$  with the signals observed in the experiments, we shall be able to exclude the initial states of the spherical harmonics that are forbidden by the dipole selection rule.<sup>45</sup>

Figure 9 illustrates normal-state angle-resolved photoemission spectra for an O<sub>2</sub>-annealed Bi(Pb)-2212 sample. The data include different geometries of photon electric-field vector and sample orientation, including (a)  $\Gamma$ - $\bar{M}$ - $Z$  oriented in the horizontal or vertical directions; (b)  $\Gamma$ - $X$  oriented in the horizontal or vertical directions; (c)  $\Gamma$ - $Y$  oriented in the horizontal or vertical directions. The insets illustrate the locations in the Brillouin zone where the spectra were obtained. The corresponding data for a He-annealed Bi(Pb)-2212 sample are illustrated in Fig. 10. For the orientation that  $\Gamma$ - $\bar{M}$ - $Z$  is horizontal or vertical, the spectra are similar to Fig. 9(a), not shown. Consequently, we can directly compare Figs. 9(b) to 10(a), and 9(c) to 10(b).

TABLE II. A list of possible  $s$ ,  $p$ , or  $d$  symmetries of the normal-state with orientations for which a normal-state band along  $\Gamma$ - $\bar{M}$ - $Z$  and  $\Gamma$ - $Y$  could (Yes) or could not (No), by symmetry, be observed.

Orientation operation symmetry	$\Gamma$ - $\bar{M}$ - $Z$		$\Gamma$ - $Y$	
	Horizontal $y \rightarrow -y$	Vertical $y \rightarrow -y$	Horizontal $x \leftrightarrow y$	Vertical $x \leftrightarrow y$
$s$	$\langle e e e \rangle$ Yes	$\langle e o e \rangle$ No	$\langle e e e \rangle$ Yes	$\langle e o e \rangle$ No
$p_x$	$\langle e e e \rangle$ Yes	$\langle e o e \rangle$ No	$\langle e e e+o \rangle$ Yes	$\langle e o e+o \rangle$ Yes
$p_y$	$\langle e e o \rangle$ No	$\langle e o o \rangle$ Yes	$\langle e e e+o \rangle$ Yes	$\langle e o e+o \rangle$ Yes
$p_z$	$\langle e e e \rangle$ Yes	$\langle e o e \rangle$ No	$\langle e e e \rangle$ Yes	$\langle e o e \rangle$ No
$d_{xy}$	$\langle e e o \rangle$ No	$\langle e o o \rangle$ Yes	$\langle e e e \rangle$ Yes	$\langle e o e \rangle$ No
$d_{x^2-y^2}$	$\langle e e e \rangle$ Yes	$\langle e o e \rangle$ No	$\langle e e o \rangle$ No	$\langle e o o \rangle$ Yes
$d_{3z^2-r^2}$	$\langle e e e \rangle$ Yes	$\langle e o e \rangle$ No	$\langle e e e \rangle$ Yes	$\langle e o e \rangle$ No
$d_{yz}$	$\langle e e o \rangle$ No	$\langle e o o \rangle$ Yes	$\langle e e e+o \rangle$ Yes	$\langle e o e+o \rangle$ Yes
$d_{xz}$	$\langle e e e \rangle$ Yes	$\langle e o e \rangle$ No	$\langle e e e+o \rangle$ Yes	$\langle e o e+o \rangle$ Yes
Experiment				
O <sub>2</sub> Bi(Pb)-2212	Yes	No	No	Yes
He Bi(Pb)-2212	Yes	No	No	No

Several important points emerge from the data of Figs. 9 and 10. Both types of samples exhibit the same symmetry (even symmetry) for the state along the  $\Gamma$ - $M$ - $Z$  direction. However, there is a change of symmetry for the state along the  $\Gamma$ - $X$  direction. O<sub>2</sub>-annealed samples exhibit a state of mixed (even and odd) symmetry along  $\Gamma$ - $X$ . By contrast, He-annealed samples exhibit a state of odd symmetry along  $\Gamma$ - $X$ . In addition, there is a change of symmetry for the state along the  $\Gamma$ - $Y$  direction. For O<sub>2</sub>-annealed samples, the state along  $\Gamma$ - $Y$  exhibits odd symmetry [note the strong dispersing peak in the vertical orientation, Fig. 9(c)]. This strong, dispersing, peak along  $\Gamma$ - $Y$  is not observed in either orientation for He-annealed samples [Fig. 10(c)].

We have compared the data in Figs. 9 and 10 to the symmetry of various spherical harmonics.<sup>44</sup> A similar analysis has been performed earlier by Kelley *et al.*<sup>46</sup> for the superconducting state of Bi-2212 and by Ratner *et al.*<sup>47</sup> for Pr-doped Bi<sub>2</sub>Sr<sub>2</sub>CuO<sub>6+y</sub>. We have assumed that the coupling between the photon electric field and the near  $E_f$  states along the  $c$  axis is so weak that the term  $P_z A_z$  in the dipole interaction can be ignored.<sup>44,47</sup> Tables I and II present the comparison between experimental data of the states along the  $\Gamma$ - $X$ ,  $\Gamma$ - $Y$ , and  $\Gamma$ - $M$ - $Z$  directions to various spherical harmonics. For O<sub>2</sub>-annealed Bi(Pb)-2212 samples the symmetry of the states along  $\Gamma$ - $X$  is consistent only with either  $p_x$  or  $d_{xz}$  spherical harmonic, while the states along  $\Gamma$ - $Y$  are consistent

with only a  $d_{x^2-y^2}$  spherical harmonic. For He-annealed Bi(Pb)-2212 samples, the states along  $\Gamma$ - $X$  are consistent with a  $d_{x^2-y^2}$  spherical harmonic, while the states along the  $\Gamma$ - $Y$  direction are not consistent with any single spherical harmonic.

The data of Figs. 9 and 10 establish that varying the oxygen stoichiometry changes the symmetry of the normal-state dispersing wave function along both the  $\Gamma$ - $X$  and  $\Gamma$ - $Y$  directions. The data were taken in the normal state, so, within a one electron picture, Bloch's theorem applies. Consequently, a change in symmetry is due to a change in the spatial orientation of the wave function. We have looked for, and found no indication of, a change in the structure of the CuO<sub>2</sub> planes. We have, however, observed a change in the interlayer coupling (Fig. 3). In the absence of a structural change in the CuO<sub>2</sub> planes, the data compel us to conclude that the change in wavefunction symmetry is caused by the change in interlayer coupling.

The above conclusion is within the context of a one-electron picture, for which Bloch's theorem holds. However, as we mention earlier, Dagotto, Nazarenko, and Boninsegni<sup>43</sup> recently obtained quantitative agreement with our data<sup>19</sup> for the Bi-2212 system. Reference 43 argues that the dispersion relations arise from many-body effects, within the context of a  $t$ - $J$  model. Calculations are in progress to extend these results by including next-nearest-neighbor interactions.<sup>48</sup> At present, we are un-

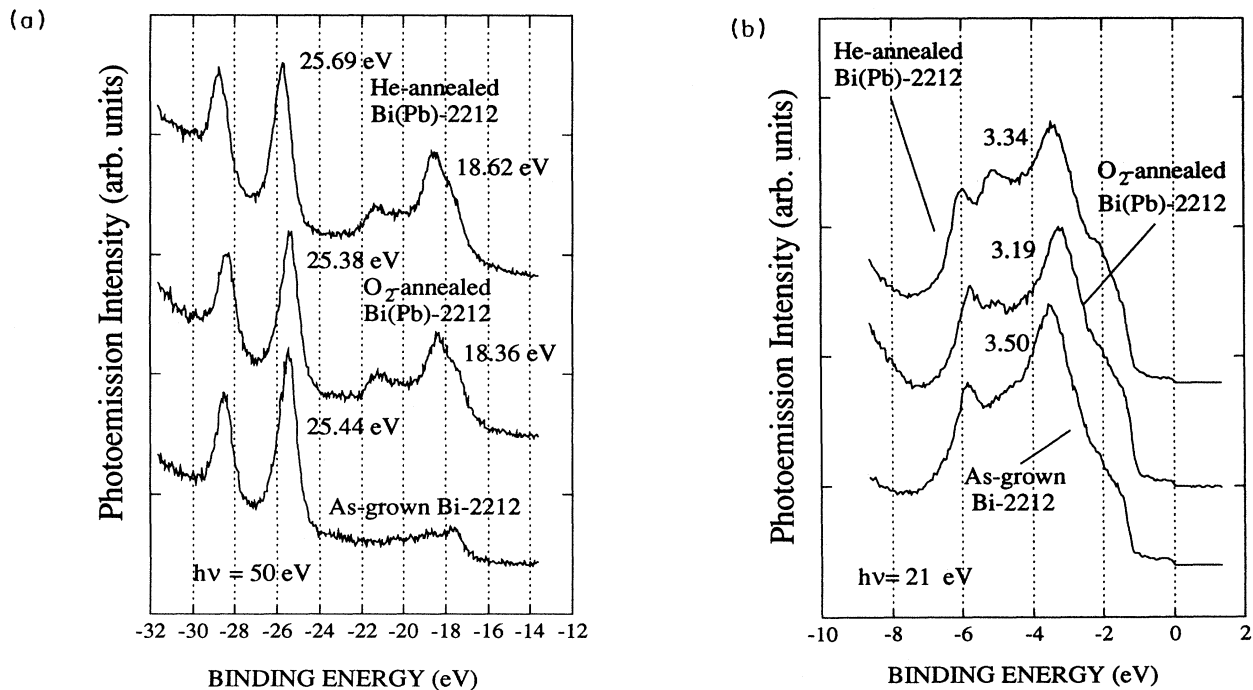


FIG. 11. (a) The Bi(5d) core levels for as-grown Bi-2212 ( $T_c = 90$  K), the Bi(5d) and Pb(5d) core levels for O<sub>2</sub>-annealed Bi(Pb)-2212 ( $T_c = 75$  K), and He-annealed Bi(Pb)-2212 ( $T_c = 85$  K). The binding energies are labeled nearby the core level peaks. The photon energy  $h\nu$  is 50 eV. (b) The valence spectra for undoped Bi-2212 ( $T_c = 90$  K) and O<sub>2</sub>-annealed Bi(Pb)-2212 ( $T_c = 75$  K) and He-annealed Bi(Pb)-2212 ( $T_c = 85$  K). Notice the shifts of main feature which consists of mostly Cu(3d) valence. The photon energy  $h\nu = 21$  eV is used. We emphasize that the core levels and valence spectra were taken on the same sample of different materials. Only the photon energy of the monochromator is different.

aware of any available many-body calculation to which we can compare our data.

## VI. Bi(5*d*) AND Pb(5*d*) CORE LEVELS

As noted earlier, one motivation for our study was the earlier results of Olson and colleagues,<sup>16</sup> which did not appear consistent with a rigid-band picture. Other investigators<sup>18</sup> have also argued that a rigid-band picture is inappropriate for the cuprate superconductors. The change in wave-function symmetry along  $\Gamma$ - $X$  and  $\Gamma$ - $Y$ , as concluded in the preceding section, are also inconsistent with a two-dimensional, rigid-band picture. We used another method to determine whether a rigid-band model is appropriate. In the rigid-band model, changing the oxygen stoichiometry (the carrier concentration) will change the chemical potential. Such a change of chemical potential would produce a rigid shift of all electronic states, including the valence band and core levels.

We thus measured the valence band and Bi(5*d*) core levels for three types of samples: as-grown Bi-2212 ( $T_c = 90$  K), O<sub>2</sub>-annealed Bi(Pb)-2212 ( $T_c = 75$  K), and He-annealed Bi(Pb)-2212 ( $T_c = 85$  K). Figure 11 illustrates the results. The data in Fig. 11 are inconsistent with a rigid-band model. We first used the as-grown Bi-2212 samples as a reference. The conduction band of the O<sub>2</sub>-annealed Bi(Pb)-2212 samples were shifted by 310 meV to lower binding energy. However, the Bi(5*d*) core levels of the same samples were shifted by only 60 meV to lower binding energy. For the He-annealed Bi(Pb)-2212 samples, the conduction band was shifted by 160 meV to lower binding energy, while the Bi(5*d*) core levels were shifted by 250 meV to higher binding energy. Thus, the rigid-band model, which would result in the same shift of all states, is inconsistent with the data.

In addition, the rigid-band model is also inconsistent with the data taken from only lead-doped samples. As Fig. 11 illustrates, we also measured the Pb(5*d*) core level for such samples. Using O<sub>2</sub>-annealed Bi<sub>1.6</sub>Pb<sub>0.4</sub>Sr<sub>2</sub>CaCu<sub>2</sub>O<sub>8+x</sub> samples as a reference, the shifts of the He-annealed Bi<sub>1.6</sub>Pb<sub>0.4</sub>Sr<sub>2</sub>CaCu<sub>2</sub>O<sub>8+x</sub> samples include the valence band (150 meV higher binding energy), the Bi(5*d*) core level (310 meV higher binding energy), and the Pb(5*d*) core level (260 meV higher bind-

ing energy).

In summary, we do observe a shift of the chemical potential to lower absolute energy for O<sub>2</sub>-annealed samples, as expected. However, the rigid-band model is not consistent with our data.

## VII. CONCLUSIONS

From our TEM data, we have demonstrated that Bi<sub>1.6</sub>Pb<sub>0.4</sub>Sr<sub>2</sub>CaCu<sub>2</sub>O<sub>8+x</sub> is structurally orthorhombic and its crystal structure is not sensitive to oxygen stoichiometry we applied. However, we have observed a large reduction in *c*-axis resistivity for O<sub>2</sub>-annealed Bi<sub>1.6</sub>Pb<sub>0.4</sub>Sr<sub>2</sub>CaCu<sub>2</sub>O<sub>8+x</sub> samples, consistent with earlier reports. The Fermi surface of such samples exhibits orthorhombic symmetry, incomplete Fermi-surface nesting, and a pocket around the  $\bar{M}$  point (which seems absent for He-annealed samples).

In addition, there is a change in the symmetry of the normal-state dispersing band along both the  $\Gamma$ - $X$  and  $\Gamma$ - $Y$  directions with oxygen stoichiometry. Within the one-electron band-structure picture, the data indicate that the change in symmetry is caused by the change in inter-layer coupling as indicated by the change of *c*-axis resistivity.

By measuring the shift in both the chemical potential (valence band) and core levels, we have established that the rigid-band picture does not apply to the Bi<sub>1.6</sub>Pb<sub>0.4</sub>Sr<sub>2</sub>CaCu<sub>2</sub>O<sub>8+x</sub> system, consistent with earlier reports on other cuprate systems.

## ACKNOWLEDGMENTS

We benefited from discussions with David Larbaestier and his critical reading of the manuscript. Conversations with Elbio Dagotto and results prior to publication are acknowledged. C. Quitmann kindly provided technical assistance. We acknowledge the financial support provided by the U.S. NSF, both directly (Grant No. DMR-9214707) and through support of the Synchrotron Radiation Center (SRC, Grant No. DMR-9212658), by Ecole Polytechnique Fédérale Lausanne and the Fonds National Suisse de la Recherche Scientifique.

<sup>1</sup> J.C. Campuzano, G. Jennings, M. Faiz, L. Beaulaigue, B.W. Veal, J.Z. Liu, A.P. Paulikas, K. Vandervoort, H. Claus, R.S. List, A.J. Arko, and R.J. Bartlett, *Phys. Rev. Lett.* **64**, 2308 (1990).

<sup>2</sup> J. Tobin, C.G. Olson, C. Gu, J.Z. Liu, F.R. Solabli, M.J. Fluss, R.H. Howell, J.C. O'Brien, H.B. Radousky, and P.A. Sterne, *Phys. Rev. B* **45**, 5563 (1992).

<sup>3</sup> R. Liu, B.W. Veal, A.P. Paulikas, J.W. Downey, H. Shi, C.G. Olson, C. Gu, A.J. Arko, and J.J. Joyce, *Phys. Rev. B* **45**, 5614 (1992).

<sup>4</sup> R. Liu, B.W. Veal, A.P. Paulikas, J.W. Downey, P.J. Kostić, S. Fleshler, U. Welp, C.G. Olson, X. Wu, A.J. Arko, and J.J. Joyce, *Phys. Rev. B* **46**, 11 056 (1992).

<sup>5</sup> S. Massidda, J. Yu, A.J. Freeman, and D.D. Koelling, *Phys. Lett. A* **122**, 198 (1987).

<sup>6</sup> J. Yu, S. Massidda, A.J. Freeman, and D.D. Koelling, *Phys. Lett. A* **122**, 203 (1987).

<sup>7</sup> W.E. Pickett, R.E. Cohen, and H. Krakauer, *Phys. Rev. B* **42**, 8764 (1990).

<sup>8</sup> K. Gofron, J.C. Campuzano, H. Ding, C. Gu, R. Liu, B. Dabrowski, B.W. Veal, W. Cramer, and G. Jennings, *J. Phys. Chem. Solids* **54**, 1193 (1993).

<sup>9</sup> A.A. Abrikosov, J.C. Campuzano, and K. Gofron, *Physica C* **214**, 73 (1993).

<sup>10</sup> J.D. Jorgensen, S. Pei, P. Lightfoot, H. Shi, A.P. Paulikas, and B.W. Veal, *Physica C* **167**, 671 (1990).

- <sup>11</sup> H. Claus, S. Yang, A.P. Paulikas, J.W. Downey, and B.W. Veal, *Physica C* **171**, 205 (1990).
- <sup>12</sup> B.W. Veal, A.P. Paulikas, H. You, H. Shi, Y. Fang, J.W. Downey, *Phys. Rev. B* **42**, 6305 (1990).
- <sup>13</sup> B. Koch, H.P. Geserich, and T. Wolf, *Solid State Commun.* **71**, 495 (1989).
- <sup>14</sup> S. Massidda, J. Yu, and A.J. Freeman, *Physica C* **152**, 251 (1988).
- <sup>15</sup> H. Krakauer and W.E. Pickett, *Phys. Rev. Lett.* **60**, 1665 (1988).
- <sup>16</sup> C.G. Olson, R. Liu, D.W. Lynch, R.S. List, A.J. Arko, B.W. Veal, Y.C. Chang, P.Z. Jiang, and A.P. Paulikas, *Phys. Rev. B* **42**, 381 (1990).
- <sup>17</sup> B.O. Wells, Z.-X. Shen, D.S. Dessau, W.E. Spicer, C.G. Olson, D.B. Mitzi, A. Kapitulnik, R.S. List, and A. Arko, *Phys. Rev. Lett.* **65**, 3056 (1990).
- <sup>18</sup> A.Q. Pham, F. Studer, N. Merrien, A. Maignan, C. Michel, and B. Raveau, *Phys. Rev.* **48**, 1249 (1993).
- <sup>19</sup> Jian Ma, C. Quitmann, R.J. Kelley, P. Alm eras, H. Berger, G. Margaritondo, and M. Onellion, *Phys. Rev. B* (to be published).
- <sup>20</sup> D. Dessau, Z.-X. Shen, D.M. King, D.S. Marshall, L.W. Lombardo, P.H. Dickinson, A.G. Loeser, J. DiCarlo, C.-H. Park, A. Kapitulnik, and W.E. Spicer, *Phys. Rev. Lett.* **71**, 2781 (1993).
- <sup>21</sup> J. Osterwalder, P. Aebi, P. Schwaller, L. Schlapbach, M. Shimoda, T. Mochiku, and K. Kadowaki, *Appl. Phys. A, Surf. Sci.* (to be published).
- <sup>22</sup> C. Kendziora, M.C. Martin, J. Hartge, L. Mihaly, and L. Forro, *Phys. Rev. B* **48**, 3531 (1993).
- <sup>23</sup> S.A. Sunshine, T. Siegrist, L.F. Schneemeyer, D.W. Murphy, R.J. Cava, B. Batlogg, R.B. van Dover, R.M. Fleming, S.H. Glarum, S. Nakahara, R. Farrow, J.J. Krajewski, S.M. Zahurak, J.V. Waszczak, J.H. Marshall, P. Marsh, L.W. Rupp, and W.F. Peck, *Phys. Rev. B* **38**, 893 (1988).
- <sup>24</sup> R. Ramesh, M.S. Hegde, C.C. Chang, J.M. Tarascon, S.M. Green, and H.L. Luo, *J. Appl. Phys.* **66**, 4878 (1989).
- <sup>25</sup> O. Eibl, *Physica C* **175**, 419 (1991).
- <sup>26</sup> Chen Xianhui, Qian Yitai, Chen Zuyao, Lin Chun, Yang Li, Mao Ziqiang, and Zhang Yuheng, *Phys. Rev. B* **46**, 9181 (1992).
- <sup>27</sup> Chen Xianhui, Xu Cheng, Cao Liezhao, and Chen Zhaojia, *Physica C* **208**, 38 (1993).
- <sup>28</sup> N. Fukushima, H. Niu, S. Nakamura, S. Takeno, M. Hayashi, and K. Ando, *Physica C* **159**, 777 (1989).
- <sup>29</sup> M. Weber, A. Amato, F.N. Gygax, A. Schenck, H. Maletta, V.N. Duginov, V.G. Grebinnik, A.B. Lazarev, V.G. Olshchovsky, V.Y. Pomjakushin, S.N. Shilov, V.A. Zhukov, B.F. Kirillov, A.V. Pirogov, A.N. Ponomarev, V.G. Storchak, S. Kapusta, and J. Bock, *Phys. Rev. B* **48**, 13 022 (1993).
- <sup>30</sup> F.X. R egi, J. Schneck, H. Savary, C. Dagu et, and F. Huet, *IEEE Trans. Appl. Supercond.* **3**, 1190 (1993).
- <sup>31</sup> X.L. Wu, Z. Zhang, Y.L. Wang, and C.M. Lieber, *Science* **248**, 1211 (1990).
- <sup>32</sup> H. Berger (unpublished).
- <sup>33</sup> Y. Matsui, S. Takekawa, S. Horiuchi, K. Shoda, A. Umezono, S. Nakamura, and C. Tsuruta, *J. Electron Microsc.* **39**, 223 (1990).
- <sup>34</sup> K.K. Fung, C.Y. Yang, and Y.F. Yan, *Appl. Phys. Lett.* **55**, 280 (1989).
- <sup>35</sup> C.H. Chen, D.J. Werder, G.P. Espinosa, and A.S. Cooper, *Phys. Rev. B* **39**, 4686 (1989).
- <sup>36</sup> C.J. Humphreys, D.J. Eaglesham, D.M. Maher, and H.L. Fraser, *Ultramicroscopy* **26**, 13 (1988).
- <sup>37</sup> P. Goodman, P. Miller, T.J. White, and R.L. Withers, *Acta Crystallogr. B* **48**, 376 (1992).
- <sup>38</sup> For a review, see B. Batlogg, *Physica B* **169**, 7 (1991).
- <sup>39</sup> X.Y. Cai *et al.* (unpublished).
- <sup>40</sup> P. Aebi, J. Osterwalder, P. Schwaller, L. Schlapbach, M. Shimoda, T. Mochiku, and K. Kadowaki, *Phys. Rev. Lett.* **72**, 2757 (1994).
- <sup>41</sup> R.J. Kelley, Jian Ma, M. Onellion, M. Marsi, P. Alm eras, H. Berger, and G. Margaritondo, *Phys. Rev. B* **48**, 3534 (1993).
- <sup>42</sup> J. Ruvald, C.T. Rieck, and A. Virosztek, *Phys. Rev. B* (to be published).
- <sup>43</sup> E. Dagotto, A. Nazarenko, and M. Boninsegni, *Phys. Rev. Lett.* **73**, 728 (1994).
- <sup>44</sup> E.W. Plummer and W. Eberhardt, *Adv. Chem. Phys.* **49**, 533 (1982).
- <sup>45</sup> J. Hermanson, *Solid State Commun.* **22**, 9 (1977).
- <sup>46</sup> R.J. Kelley, Jian Ma, G. Margaritondo, and M. Onellion, *Phys. Rev. Lett.* **71**, 4051 (1993).
- <sup>47</sup> E.R. Ratner, Z.-X. Shen, D.S. Dessau, B.O. Wells, D.S. Marshall, D.M. King, W.E. Spicer, J.L. Peng, Z.Y. Li, and R.L. Greene, *Phys. Rev. B* **48**, 10 482 (1993).
- <sup>48</sup> E. Dagotto (private communication).

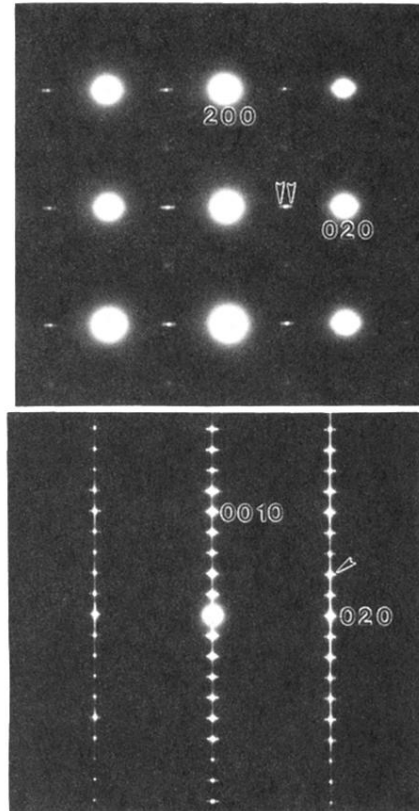


FIG. 1. The [001] (a) and [100] (b) electron-diffraction patterns (EDP) of the oxygen-annealed Bi(Pb)-2212 single-crystal samples. Diffraction spots are indexed based on the fundamental structure. Satellite spots, as indicated by arrows, are due to the modulated structure. Similar EDP were observed on the helium-annealed Bi(Pb)-2212 single-crystal samples.

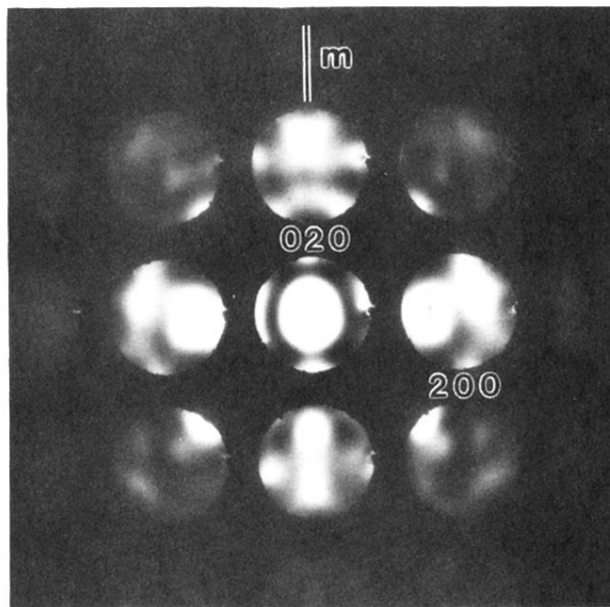


FIG. 2.  $[001]$  Convergent beam electron-diffraction (CBED) pattern of the oxygen-annealed Bi(Pb)-2212 single-crystal samples. The pattern has only one mirror plane as indicated by the vertical line marked  $m$ , implying a  $2mm$  point-group symmetry of orthorhombic structure. A similar CBED pattern was observed on the helium-annealed Bi(Pb)-2212 single-crystal samples.